Air Entrainment in Gas Burners

G. VON ELBE AND J. GRUMER

Central Experiment Station, U. S. Bureau of Mines, Pittsburgh, Pa.

Air entrainment in burners with cylindrical tubes can be calculated on the basis that part of the stream momentum is transformed into static pressure corresponding to the flow resistance imposed by friction, buoyancy, and flame thrust. Satisfactory agreement is found with experimental data. When the flame is to be distributed over a number of port openings, Venturi ducts are required. The energy loss in a Venturi duct has been studied by separately measuring the potential energy, the kinetic energy corresponding to average velocity, and the kinetic energy contributed by the velocity profile. It has been concluded that between the Venturi throat and the burner head, the latter contribution is lost in the form of eddy motions.

THE problem of primary air entrainment in atmospheric gas burners has been treated in many publications of the National Bureau of Standards and the American Gas Association Testing Laboratories (*2, 3, 5-7, 11*). The factors of the burner design which have been studied comprise: the slope, length, and throat diameter of the Venturi tube, shape of the Venturi inlet, bends in the Venturi tube, the total port area, the geometrical design of the burner head, the size and depth of the portholes, internal surface conditions, primary air inlets, orifice position, and area. The variables of fuel gas that have been studied comprise: specific gravity, heating value, pressure, and burner temperature. The air entrainment has been represented in general by an equation of the form

Stream momentum at orifice = $k \times$ stream momentum at port

where the coefficient k is empirically determined as a function of the above variables. The basic units of mass and velocity are customarily converted to units of gas pressure, heating value, specific gravity, and burner temperature to meet the needs of the gas engineer. The validity of these relations is necessarily restricted and it is desirable to obtain a closer theoretical insight into the process of air entrainment. Moreover, it appears that systematic data on air entrainment are available only for burners with Venturi ducts and that, except for data on flash tube performance (*4*) which are not applicable here, no systematic data on cylindrical burner tubes are available.

This paper deals with burners consisting of a free gas jet in air and either a cylindrical burner tube or a Venturi duct which leads to a manifold of small flame ports.

CYLINDRICAL BURNER TUBES

Figure 1 illustrates the theory for burners of this type; similar considerations apply to air injection ventilators (*16, 19*). The gas stream forms a free jet between the plane, o, of the orifice and some plane, x, and the stream cross section expands due to air entrainment from A_o at the orifice to A_x in plane x. Assuming that the mixing process is completed in plane x and that the temperature does not change appreciably along the duct, then, because the gas may be treated as an incompressible fluid, the density, ρ, and the volumetric flow, V, of the gas-air mixture remain constant from plane x on to the end of the burner tube. The static pressure within the free jet is the same as that of the surrounding atmosphere (*8*) but downstream from plane x the static pressure must increase until it is sufficiently large to overcome the wall friction in the tube and the back pressure of the flame. This can only come about by a decrease of momentum, and correspondingly, the stream cross section expands between plane x and some plane m from A_x to the full cross section, A, of the tube with a decrease of the average gas velocity from V/A_x to V/A. In other words, between planes x and m the gas velocity profile is redistributed over the area, A. In this process some stream energy is lost in the form of eddies (*9*).

At m the gas stream attains the maximum static pressure p_m above atmospheric. The force acting between planes m and x is Ap_m as the static pressure in plane x is evidently atmospheric over the whole area A. This force is equal to the loss of momentum per unit time between x and m—that is, $Ap_m = I_x - I_m$. I denotes the momentum crossing a plane per unit time, or momentum flux, and its value in some plane, y, is the integral, $\int_0^{A_y} \rho u^2 dA$, over the stream cross section, A_y: u is the velocity in the cross-sectional element dA.

DEFINITIONS AND SYMBOLS. Through dA flow in unit time mass $\rho u dA$, momentum $\rho u^2 dA$, and kinetic energy $\frac{1}{2}\rho u^3 dA$. For a steady stream of nonuniform velocity, $\bar{u}$, over cross section A_y, and another stream of uniform velocity, $\bar{u}$, and the same cross section, the mass flows ρV_y and ρV are $\rho \int_0^{A_y} u dA$ and $\rho \bar{u} A_y$, respectively. If the flows and densities are the same for both streams one obtains further

$$\rho V_y - \rho V = \rho \bar{u} A_y \int_0^{A_y} \left(\frac{u}{\bar{u}} - 1\right) \frac{dA}{A_y} = 0,$$

but the corresponding differences of momentum flux and kinetic energy flux, $I_y - I = \rho \bar{u}^2 A_y \int_0^{A_y} \left[\left(\frac{u}{\bar{u}}\right)^2 - 1\right] \frac{dA}{A_y}$, and $E_y - E = \frac{1}{2} \rho \bar{u}^3 A_y \int_0^{A_y} \left[\left(\frac{u}{\bar{u}}\right)^3 - 1\right] \frac{dA}{A_y}$, respectively, are always positive; in addition, the integral in the second term is larger than the integral in the first term. The principle involved here can be stated in the general form:

If an integral, $\int_{x_1}^{x^2} (y - 1) dx$, is zero, $\int_{x_1}^{x^2} (y^n - 1) dx$ is

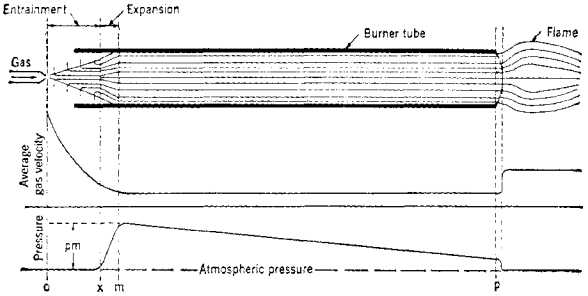

Figure 1. Scheme of Air Entrainment for Cylindrical Burner Tube

positive for $n > 1$ and increases as the exponent, n, is increased. The terms in front of the integral signs are I and E, respectively. Introducing $\iota_y = I/I_y$ and $\epsilon_y = E/E_y$, the two integral factors become $(1/\iota_y) - 1$ and $(1/\epsilon_y) - 1$, and from the foregoing, $\iota_y > \epsilon_y$. For parabolic velocity distribution one obtains $\iota = 0.75$ and $\epsilon = 0.5$.

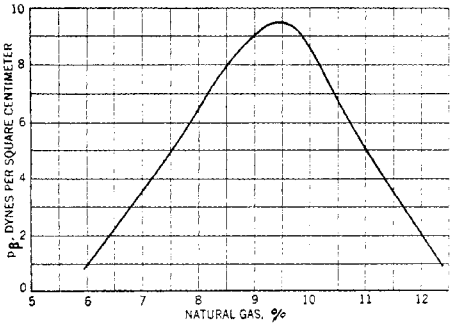

Figure 2. Flame Pressure Curve for Natural Gas-Air Mixtures

The difference, $E_y - E$, evidently represents the contribution of the velocity profile to the energy flux. Another contribution is the potential energy due to the static pressure difference, p, between plane y and the atmosphere. Its magnitude in any cross-sectional element is $pudA$ per unit time, as is shown in the derivation of Bernoulli's theorem. As the static pressure is generally constant over the stream cross section, the total contribution becomes $p\int_0^{A_y} udA = pV$. The energy flux can thus be represented as the sum of the three terms, $E + (E_y - E) + pV$, which are separately measurable. After dividing by V the sum may be written as $q = \frac{1}{2}\rho\bar{u}^2 + \frac{1}{2}\rho\bar{u}^2[(1/\epsilon) - 1] + p$, where each term has the dimension of pressure.

For the special case of uniform velocity, the momentum flux becomes $\rho V^2/A_y$. This value increases when the velocity over the cross section, A_y, becomes nonuniform, even though the flow, V, remains the same. Thus, generally $I_y = \rho V^2/\iota_y A_y$, where the number $\iota_y \leq 1$ is dependent only on the distribution of velocity over the stream cross section. The larger the relative differences of the velocity vectors from the average, the smaller ι_y becomes.

The equation for the force between m and x may now be written as $A\,p_m = \rho V^2/\iota_x A_x - \rho V^2/\iota_m A$, hence

$$p_m = \frac{\rho V^2}{A}\left(\frac{1}{\iota_x A_x} - \frac{1}{\iota_m A}\right) \quad (1)$$

Between planes o and x the momentum flux, I, remains constant (*8*); this may be expressed as

$$\rho_o V_o^2/\iota_o A_o = \rho V^2/\iota_x A_x \quad (2)$$

where ρ_o is the density and V_o the flow of the fuel gas. Combining Equations 1 and 2, and transposing

$$V^2/V_o^2 = (\rho_o \iota_m A/\rho \iota_o A_o) - p_m \iota_m A^2/\rho V_o^2 \quad (3)$$

Equation 3 correlates the fuel-gas percentage $100V_o/V$ in the burner stream with the fuel-gas flow V_o from the supply.

The density, ρ, is calculated from the densities of air and fuel gas by the mixture rule

$$\rho = \rho_{air}(1 - V_o/V) + \rho_o V_o/V \quad (4)$$

The static pressure p_m in a horizontal tube is the sum of the pressures p_α due to friction at the tube wall and p_β due to the thrust of the flame gas. In vertical tubes an additional stress arises from the buoyancy of the fuel gas with corresponding terms p_γ for upright, and $-(p_\gamma)$ for downright burners.

For laminar flow, from Poiseulle's equation,

$$p_\alpha = 8VL\eta/\pi a^4 = 8\pi VL\eta/A^2 \quad (5)$$

L is the length of the tube, a the radius, and η the viscosity of the mixture. For turbulent flow (*10*)

$$p_\alpha = (L\rho V^2/2aA^2)\,[0.0036 + 0.24(2\ R)^{0.38}] \quad (5a)$$

where Reynolds number $R = 2V\rho/\pi a\eta$. The viscosity η is calculated from

$$\eta = \eta_{air}(1 - V_o/V) - \eta_o V_o/V \quad (6)$$

The pressure p_β is calculated from the equation (*13*)

$$p_\beta = S_u^2[(\rho_u/\rho_b) - 1] \quad (7)$$

where the burning velocity S_u and the flame-gas density ρ_b are functions of mixture composition. For the natural gas used in the present investigation, S_u and ρ_b are known as functions of the fuel : air ratio from previous work (*14*, *15*) and have been used to calculate the curve of p_β in Figure 2. The pressure p_γ is calculated from

$$p_\gamma = gL(\rho_{air} - \rho) \quad (8)$$

where g is the gravitation constant.

The coefficients ι_o and ι_m must be determined experimentally. This is done simply by determining the values that give the closest agreement between calculated and experimental air entrainment. The direct determination from measurements of the velocity distribution would be rather difficult in this case and also hardly worthwhile because the general trend of the theoretical air entrainment curves is not significantly changed by any reasonable choice of the ι-coefficients.

Another parameter that must be determined experimentally is the proper distance between the gas orifice and the entrance to the burner tube. If the orifice approaches the burner tube too closely, air entrainment is throttled; if it is too far away, the entrainment is increased but the jet cross section exceeds the tube cross section and a part of the gas mixture flows around the burner. Experimentally it is found that over an appreciable range of distance the orifice is neither too close nor too far away, and the air entrainment remains constant.

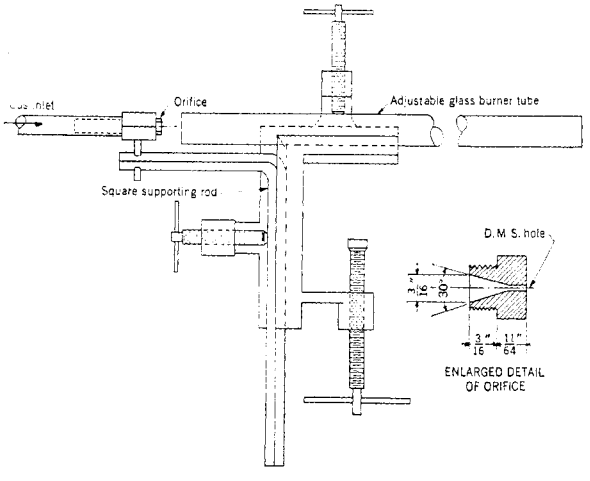

Figure 3. Clamp for Orifice and Burner Tube

The burners used in these experiments consisted of glass tubes of uniform diameter and brass orifices of the fixed type having a 15° angle of approach to the drill hole (*1*). Drill manufacturers' sizes 1/32, 62, 59 were used. Tubes and orifices were held together by a clamp, as shown in Figure 3. The orifice could be accurately centered at any desired distance from the tube entrance and the burner could be mounted in any position. Natural gas from the gas line was used for these experiments. Its composition was

frequently checked and remained sufficiently constant for the duration of these experiments. The gas averaged 81.1% methane, 18.0% ethane, 0.5% propane to pentane, and 0.4% nitrogen. This corresponds to a specific gravity of 0.65 and a viscosity, at 25° C., of 1.08×10^{-4} poise, calculated from data of the constituents (*12, 18*).

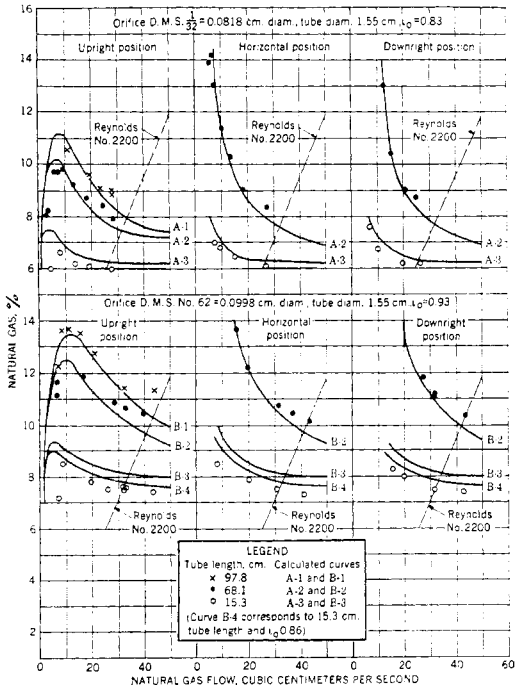

Figure 4. Effect of Length and Position of Cylindrical Burner Tubes on Air Entrainment

Calculated curves and experimental points. Burner not lighted; natural gas, $\rho_0/\rho = 0.65$ η_0 1.08×10^{-4} poise; air, $\rho_{air} = 11.5 \times 10^{-4}$ g./cc. $\eta_{air} = 1.83 \times 10^{-4}$ poise

The gas flow was measured by flowmeters. Samples of the gas-air mixture were taken through a side arm near the end of the tube without obstructing the gas flow. The sampling rate was adjusted to about 1% of the total flow using a mercury-filled sampling bottle. The gas percentage of the sample was determined in a thermal conductivity apparatus (*17*) with gas-conductivity cells furnished by the National Bureau of Standards.

Figure 4 shows calculated curves and experimental data for unlighted burners in various positions. The flow through the burner tube is generally considerably below the critical Reynolds number and p_a is therefore calculated for laminar flow. This assumption is not strictly valid because some jet turbulence persists for an appreciable distance down the tube, particularly in short tubes and at high gas velocities. On the other hand, this is somewhat compensated by the fact that under such conditions the contribution of friction is smallest. The curves for upright burners pass through a maximum because of the opposing effects of buoyancy and friction. In downright burners buoyancy and friction augment each other; this results in lower air entrainment—that is, in higher gas percentages—than for horizontal burners where only friction is acting. With increasing gas flow, the second term of Equation 3 vanishes for the laminar case but not (Equation 5a) for the turbulent case. Correspondingly, for flows near the critical Reynolds number of 2200, the experimental gas percentages are higher than the theoretical, particularly for long tubes where friction matters most. That this may be attributed to the transition from predominantly laminar to turbulent flow is further shown in Figure 5 by the manner in which the experimental points follow or deviate from the curves calculated for the laminar and the turbulent case.

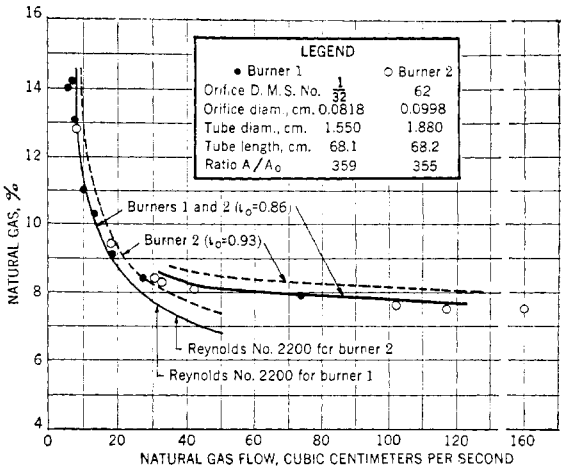

Figure 5. Cylindrical Burner Tubes—Effect of Large Reynolds Numbers on Air Entrainment

Horizontal position, burners not lighted; calculated curves and experimental points

Burners 1 and 2 of Figure 5 have different orifice and tube diameters but an almost identical ratio, A/A_o. Correspondingly, for horizontal position the experimental gas percentages coincide in the laminar flow range and almost coincide in the turbulent range as predicted by Equation 3 and the friction Equations 5 and 5a. When the burner position is changed or when the burner is lighted, the difference of the tube areas comes into effect according to Equation 3 and the flame pressure and buoyancy equations, 7 and 8, and the calculated curves and experimental points diverge (Figure 6).

For the curves of Figure 4, ι_m was chosen as 1 and ι_o as 0.83 for the smaller and 0.93 for the larger orifice. These values do not allow a good representation of the data for the shortest burner tube (curves A-3 and B-3). A close fit for all three burner lengths can be obtained by lowering the value of ι_o for each orifice and assuming large values of ι_m for short tubes and small values for long tubes. For example, by using $\iota_o = 0.86$ for the larger orifice and $\iota_m = 1$ for the short burner tube the curves B-3 become curves B-4 which fit the experimental data closely. For the longer tubes and the same orifice, the values $\iota_o = 0.86$ and $\iota_m = 0.85$ yield well fitting curves similar to curves B-1 and B-2. The 1.880-cm. burner in Figure 5 seems to require a large value of ι_m—namely, for $\iota_o = 0.86$, $\iota_m = 1$—particularly in the turbulent region. This may be attributable to more uniform velocity distribution in turbulent streams. In short and wide tubes jet turbulence persists more than in long and narrow tubes, so that the assumption of large values of ι_m for the former may have some physical meaning.

The effect of lighting a burner consists in decreasing the air entrainment corresponding to the magnitude of the flame pressure (Figure 2). This is illustrated in Figure 7. The diagrams also show the range of stable flame bounded by regions of flash back

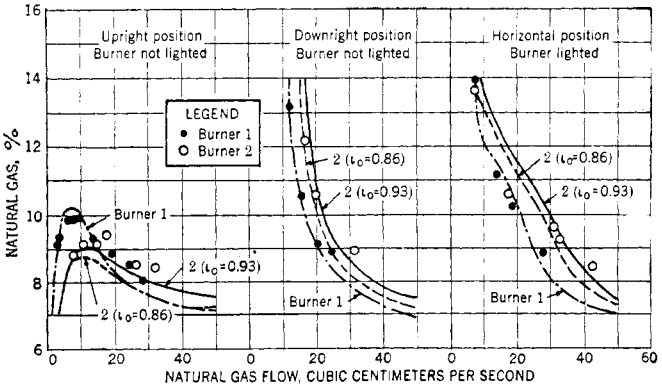

Figure 6. Effect of Nonhorizontal Position and Flame

Same burners as in Figure 5. Calculated curves and experimental points

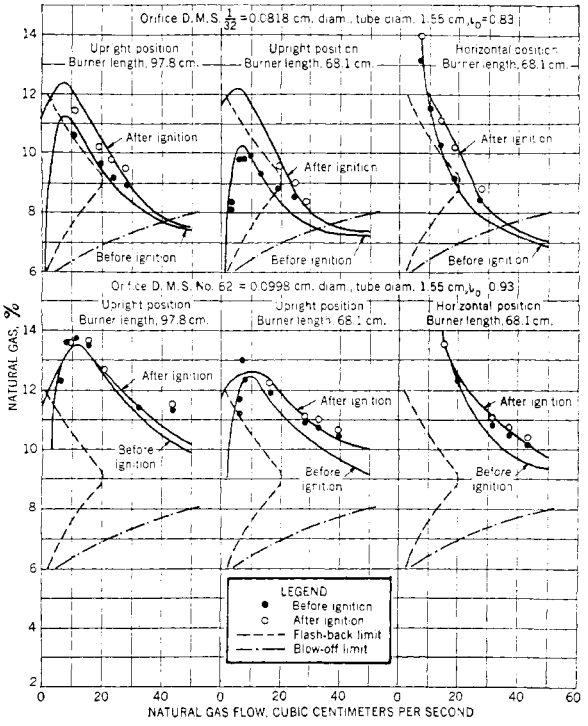

Figure 7. Effect of Ignition on Air Entrainment

Calculated curves and experimental points

and blowoff (*15*). In the case of upright position and 68.1 cm. burner length, a part of the entrainment curve for the unignited burner lies within the flash-back region. The flame pressure shifts the entrainment curve out of this region. Hence, if an attempt is made to light the burner at a flow within the flash-back region, flash back results; on the other hand, when the burner has been lighted at some higher flow it can be throttled to the same lower flow without flashing back. An example of particularly unfavorable burner characteristics is shown in Figure 8. The stable-flame region is so narrow that in practice it is not possible to light the burner—that is, the flame either flashes back or blows off. In principle, it would appear possible to maintain a

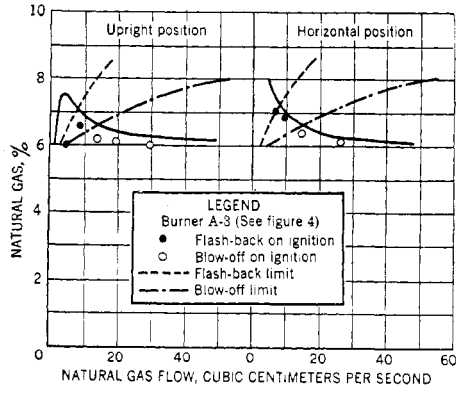

Figure 8. Burner Operating within Flame Instability

Calculated curves and experimental points

stable flame between gas flows of about 8 cc. per second to 14 cc. per second. However, the limits of flash back and blowoff shown here are accurate only for laminar flow free of fluctuations of velocity or mixture composition. In the case shown in Figure 8, the limits are actually drawn together by the residual turbulence of the jet and by fluctuations of the mixture composition inherent in the entrainment process.

The latter fluctuations merit additional discussion. Consider that in an upright lighted burner the air entrainment momentarily drops below the normal average. Then the buoyancy increases, friction decreases, and if the mixture composition is thereby shifted into the rich range—that is, past the maximum of Figure 2—the flame pressure also decreases. During the interval of these conditions in the burner tube the static pressure, p_m, remains below normal; as a consequence, the air entrainment increases above normal until the burner tube is purged of the over-rich mixture. The trend is now reversed: The air excess decreases the buoyancy; it increases the friction [due to the increased flow, V (Equation 5)] and also the flame pressure because the mixture composition is shifted back toward the stoichiometric. Hence p_m increases above normal, and the cycle repeats itself.

Such fluctuations are readily observable, particularly on long burners with appreciable purging periods. The flame cone may elongate periodically and turn green as the mixture shifts to the rich side and contract and turn blue as the trend is reversed. Under appropriate conditions the shift toward stoichiometric composition may bring the flame momentarily into the flash-back region; it then travels down the tube until it is met by the incoming over-rich mixture and swept back to the tube rim. Sometimes the incoming mixture is so over-rich that the flame is extinguished. It may be noted that flash tubes—cylindrical burners operating in the flash-back range—used for lighting a burner from a distant pilot flame, have vents or expansion chambers to release the pressure, p_m, and thus operate with constant air entrainment.

Fluctuations of the described type are not confined to upright burners but also occur in horizontal and even downright burners; the dependence of friction on mixture flow alone suffices to produce them. However, they are less strongly developed in the latter cases.

BURNERS WITH VENTURI DUCTS

When the flame is to be distributed over a number of port openings, it is necessary to transform the whole stream momentum as completely as possible into static pressure. Otherwise, the flame distribution would be uneven, the flames would be unruly due to turbulence, and considerable eddy losses would occur in the port manifold; this would reduce the air entrainment. The jet stream, therefore, enters a Venturi duct where it expands gradually before passing through the ports. As shown

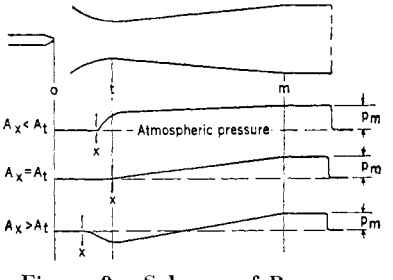

Figure 9. Scheme of Pressure Changes in Venturi Duct

in Figure 9, plane m now lies in the burner head behind the ports and plane x lies in or near the throat, depending on whether or not area A_x is equal to the throat area, A_t. The size of A_x is evidently limited by the flow of entrained air that can be pushed through the burner, and if the total port area, A, is sufficiently small, A_x becomes smaller than A_t. In this case the stream expands from A_x to A_t with eddy losses in the manner described in the previous section, and the Venturi duct is effective only during the expansion from A_t to A_m. The initial ex-

pansion from A_x to A_t increases the static pressure in the throat above atmospheric. As total port area, A, is increased, a point is reached where $A_x = A_t$, and the static pressure in the throat becomes atmospheric. Further increase of A results in $A_x > A_t$, which need not entail an appreciable loss of energy if the duct entrance forms a gradually contracting channel; in this case the stream contracts from A_x to A_t with increase of velocity and corresponding decrease of static pressure in the throat below atmospheric (*16, 19*).

If the assumptions of Bernoulli's theorem—frictionless flow and uniform velocity over the stream cross section—were valid in the Venturi duct and the ports, one could write for the case $A_x \geq A_t$, and for negligible back pressure of the flame ($p \ll p_m$),

$$\rho V^2/2A_x^2 = \rho V^2/2A_m^2 + p_m = \rho V^2/2A^2 \qquad (9)$$

hence

$$A_x = A \geq A_t$$

and combining with the free-jet equation, 2, (taking the ι-coefficients = 1) one would obtain

$$V^2/V_o^2 = \rho_o A/\rho A_o \qquad (10)$$

showing the fuel-gas percentage to be independent of flow and solely a function of the densities and the port and orifice areas.

Equation 10 can be written as:

$$I = I_o$$

where I is the stream momentum leaving the portholes. For the nonideal case, one may write accordingly

$$= kI_o$$

where $k<1$ is a function of the change of the velocity profile as the stream passes through the burner. In the literature, values of k have been determined empirically as functions of burner design variables. Such data do not permit the determination of the velocity distribution and it is accordingly difficult at this time to use the data in theoretical considerations.

The literature (*2, 7, 11*) shows this to be substantially fulfilled but furnishes little information for possible extension of the theory to the nonideal conditions which cause the actual entrainment to be lower than predicted by Equation 10.

As an approach to this problem an attempt has been made to establish the energy balance along a Venturi duct by separately measuring the three components of the energy flux, q, in the throat and the head of a test burner.

$$= \frac{1}{2}\rho\bar{u}^2 + \frac{1}{2}\rho\bar{u}^2\left((1/\epsilon) - 1\right) + p \qquad (11)$$

The first term is contributed by the kinetic energy corresponding to the average velocity, $\bar{u} = V/A_y$, the second term by the velocity profile, and the third term by the potential energy; p is the difference between the static and the atmospheric pressure.

The Venturi duct was cut into a block of maple wood according to dimensions suggested by another work (*7*). The throat diameter was $^5/_8$ inch. The inlet profile had a curvature of 3-inch radius. The duct expanded at an angle of 2° to a diameter of $1^3/_{16}$ inch. Then followed a short cylindrical section which carried a removable perforated steel plate of $^1/_4$-inch width. The perforations consisted of $^1/_8$-inch holes in hexagonal pattern. A gas-sampling tube was attached to the cylindrical head and taps were made at the head and throat for the attachment of pressure gages; care was taken to avoid any ridges protruding into the stream. The gages were of the slope type and filled with water to which a wetting agent had been added. Readings were made by means of a telescope. Pressures could also be measured by means of a slender tube which was introduced through the port to any desired point within the duct. After closing the end and cutting side holes in the tube, it served alternatively as a Pitot tube and a static tube. The accuracy of the pressure readings was about ±0.05 mm. of water. The gas orifice was aligned with the axis of the duct at variable distance from the inlet by means of a holder which permitted free air entrainment. On moving the orifice away from the throat, the air entrainment increased to a value that remained constant over some distance. The measurements were always made in this range. Other arrangements were the same as in the previous section.

Measurements were made in the throat plane and the cylindrical head section without lighting the burner. As a first step, the static throat pressure was determined for various port areas. Figure 10 shows that the throat pressure becomes zero at throat-to-port ratios of about 0.7. Further measurements were made at constant throat-to-port ratio of 0.675. The flow, V, was determined from fuel-gas flow V_o and gas-analytical value of V/V_o. The coefficient ϵ was determined from the velocity distribution as

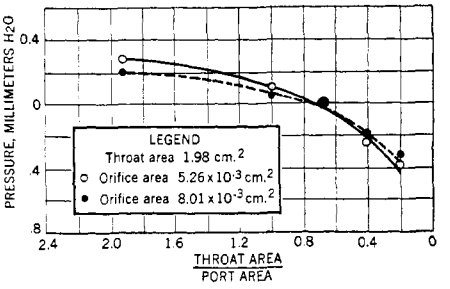

Figure 10. Static Pressures, p, at Throat for Various Port Areas

measured by means of the Pitot tube. The procedure is shown in Figure 11. From the pressure readings at various distances, r, from the axis a curve of velocity against radius is obtained from this curve, the curves for $2ur$, $2u^2r$, and $2u^3r$ are obtained and graphically integrated over the total stream radius, a. The first integral yields a value of $\bar{u}$ within the errors inherent in this method. In the calculation of $\iota = \bar{u}^2a^2/\int_0^a u^2 2\pi dr$ and $\epsilon = \bar{u}^3a^2/\int_0^a u^3 2\pi dr$, the errors cancel out to some extent. However, in Equation 11 the more accurate values of $\bar{u}$ obtained from the gas-analytical values of V have been used.

The data are summarized in Table I. Although no great accuracy can be claimed, the energy flux in the burner head is consistently found to be smaller than in the throat by an amount roughly corresponding to the contribution of the velocity profile. It appears that this part of the energy flux is lost and that the

Table I. Decrease of Energy Flux along a Venturi Duct

			Sq. Cm.			
		Head area	= 9.58			
		Throat area	= 1.98			
		Port area	= 2.93			
Orifice area, sq. cm.	5.26×10^{-3}		8.01×10^{-3}		7.83×10^{-3}	
V_o, cc./sec.	26.5		33		42.5	
V/V_o	14.9		12.7		12.6	
ρ, g./cc.	1.09×10^{-3}		1.12×10^{-3}		1.12×10^{-3}	
	Measurement at					
	Throat	Head	Throat	Head	Throat	Head
ϵ	0.55	1.0	0.64	1.0	(0.55)	1.0
$\frac{1}{2}\rho\bar{u}^2$, mm. H_2O	0.22	0.01	0.25	0.01	0.41	0.02
$\frac{1}{2}\rho\bar{u}^2\left((1/\epsilon) - 1\right)$, mm. H_2O	0.18	0.00	0.14	0.00	0.34	0.00
p, mm. H_2O	0.00	0.24	0.00	0.20	−0.06	0.35
Total, mm. H_2O	0.40	0.25	0.39	0.21	0.69	0.37
Lost between throat and head, mm. H_2O	0.15		0.18		0.32	
Contributed by the velocity profile, mm. H_2O	0.18		0.14		0.34	

stream in the duct behaves as if the velocity in the throat plane were uniform. It follows that at zero throat pressure, ratio A_t/A (throat area to port area) must equal the port discharge coefficient. This coefficient is defined by the equation, $p_m = \frac{1}{2}\rho V^2/\alpha^2 A^2$; α^2 is equal to ϵ if the only loss occurring in the efflux process is a change of the velocity profile by contraction and frictional retardation at the stream boundary. From the foregoing, however, $p_m = \frac{1}{2}\rho V^2/A_t^2$ as the kinetic energy in the burner head is very small; hence, $A_t/A = \alpha$. Values of discharge coefficients are usually found to be between 0.6 and 0.7 which appears sufficiently consistent with the observed ratio $A_t/A \sim 0.7$ at zero throat pressure.

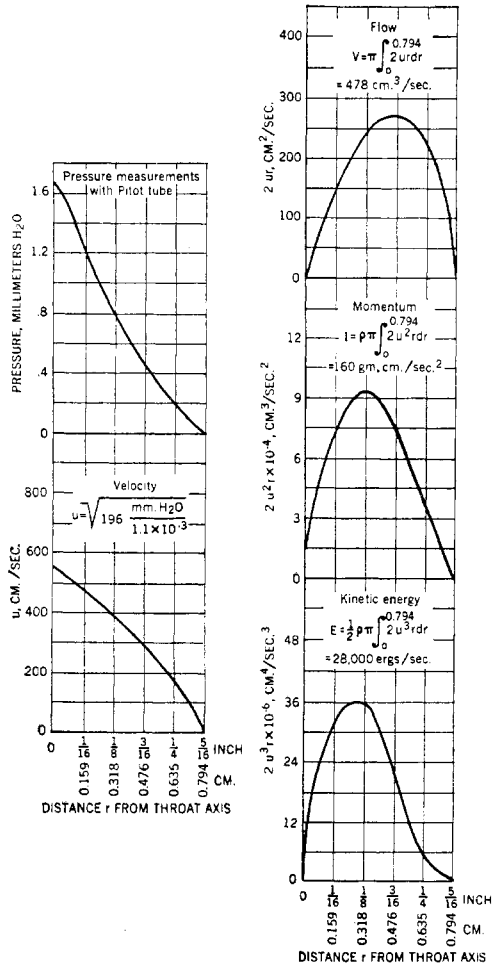

Figure 11. Pitot Tube Measurements and Derived Functions across Throat of Venturi Burner

Throat 5/16 inch = 0.794 cm; orifice area = 5.26×10^{-3} sq. cm.; throat-to-port ratio = 0.675; gas flow = 26.5 cc./sec.; $V/V_0 = 14.9$ $\rho = 1.1 \times 10^{-3}$ g./cc

The loss of the energy stored in nonuniform velocity distribution becomes understandable if one considers that the friction at the jet boundary which supports the velocity profile decreases rapidly as the stream enters the expanding duct. The velocity profile thus becomes unstable and breaks up into eddies much in the manner of a stream entering a suddenly enlarged duct.

The problem remains of establishing the energy balance between the plane x and the throat in the range of large negative and positive throat pressures, and thus to arrive at generally valid relations governing the entrainment process. It is conceivable that problems of this kind may ultimately be solved by theory, but in the absence of a theoretical treatment satisfactory answers may possibly be found by further experiments.

SUMMARY

An experimental and theoretical study has been made of the air entrainment in gas burners consisting of a free jet of fuel gas in air and either a cylindrical burner tube or a Venturi duct which leads to a manifold of small flame ports. For cylindrical burner tubes an equation of the air entrainment has been derived on the basis that part of the stream momentum is transformed into static pressure corresponding to the flow resistance imposed by friction, buoyancy, and the back thrust of the flame. The air entrainment calculated from this equation as a function of burner dimensions, burner position, and gas flow agrees well with the experimental data. Fluctuations of the air entrainment in cylindrical burners are found to be inherent in the entrainment process. Burners with Venturi ducts are required when the flame is to be distributed over a number of port openings because in this case it is necessary to transform the stream momentum as completely as possible into static pressure. In so far as the assumptions of Bernoulli's theorem are valid for the flow in the Venturi duct, an equation of the air entrainment can be readily derived. As a contribution to the study of the nonideal conditions which cause the actual entrainment to be lower than predicted, an experimental energy balance of the flow has been made between the throat and the head of a test burner. For this purpose the potential energy, the kinetic energy corresponding to average velocity, and the kinetic energy contributed by the velocity profile have been separately measured. From the data it was concluded that the latter contribution is lost between throat and head in the form of eddy motions.

NOMENCLATURE

a = radius of cross-sectional plane of burner tube, cm.
g = gravitational constant, cm. per square second.
p = static pressure difference between any cross-sectional plane of gas stream and the atmosphere, cm.
q = sum of static and velocity pressure, cm.
r = distance from axis of burner tube, cm.
u = velocity in a cross-sectional element dA, cm.
A = cross-sectional area of the gas stream, square cm.
E = kinetic energy crossing a plane per unit time, ergs per second
I = momentum crossing a plane per unit time, gram cm./per square second
L = length of burner tube, cm.
V = rate of flow of gas stream, cc. per second
α = port discharge coefficient
ϵ = kinetic energy coefficient, dependent on the degree of uniformity of the distribution of velocity over the stream cross section
ι = momentum coefficient, dependent on the degree of uniformity of the distribution of velocity over the stream cross section
η = viscosity, poise
ρ = density, grams per cc.
Su = burning velocity, cm. per second

Subscripts

b = burned gas
m = plane of maximum static pressure within burner tube
none = plane of burner ports
o = plane of fuel gas orifice
t = plane of throat of Venturi duct
x = plane where entrainment of air ceases
y = any plane of burner tube

α = refers to effect of friction at the tube walls
β = refers to effect of the thrust of the burned gas
γ = refers to effect of the buoyancy of the gas stream

LITERATURE CITED

(1) Am. Gas Assoc., "Combustion," 3rd ed., p. 110. Easton, Mack Printing Co., 1932.
(2) *Ibid.*, p. 117.
(3) Am. Gas Assoc. Testing Lab. *Bull.* **10** (March 1940).
(4) *Ibid.*, **17** (August 1943).
(5) *Ibid.*, **26** (May 1944).
(6) *Ibid.*, **37** (September 1945).
(7) Berry, W. M., Brumbaugh, I. V., Moulton, G. F., and Shawn, G. B., *Natl. Bur. Standards*, Tech. *Paper* **193** (September 1921).
(8) Ewald, P. P., Pöschl, Th., and Prandtl, L., "Physics of Solids and Fluids," 2nd ed., p. 254, London, Blachie and Son, 1936.
(9) *Ibid.*, p. 226.
(10) *Ibid.*, p. 277.
(11) Kowalke, O. L., and Ceaglske, N. H., *Am. Gas Assoc. Proc.*, 662–86 (1929).
(12) Landolt-Börnstein, "Physikalisch-chemische Tabellen," Sup. Vol. 1, p. 143; Sup. Vol. 2, p. 137, Berlin, J. Springer.
(13) Lewis, B., and von Elbe, G., "Combustion, Flames and Explosions of Gases," p. 203, Cambridge. Cambridge University Press, 1938.
(14) *Ibid.*, p. 342.
(15) Lewis, B., and von Elbe, G., *J. Chem. Phys.*, **11**, 75 (1943).
(16) McElroy, G. E., *Mining Technol.*, July 1945.
(17) Palmer, P. E., and Weaver, E. R., *Natl. Bur. Standards, Tech. Paper* **249** (Jan. 1924).
(18) Smith, M. L., and Hanson, G. H., *Oil Gas J.*, **44**, 119 (1945).
(19) Weeks, W. S., *Eng. Mining J.*, **138**, 196–9 (1937).

RECEIVED April 28, 1947. Presented before the Division of Gas and Fuel Chemistry at the 111th Meeting of the AMERICAN CHEMICAL SOCIETY, Atlantic City, N. J. Published by permission of the Director, U. S. Bureau of Mines, Department of the Interior.

Properties and Uses of Alkanesulfonic Acids

W. A. PROELL, C. E. ADAMS, AND B. H. SHOEMAKER
Standard Oil Company (Indiana), Whiting, Ind.

The alkanesulfonic acids ($C_nH_{2n+1}SO_3H$) have been known for many years; their preparation and some of the properties of various members of the series have been described in the literature from time to time. An excellent review of previous work on the chemistry of these acids is given by Suter (*8*). Although a few of the alkanesulfonic acids of higher molecular weight have been produced for some time on a commercial scale for use as surface active agents, alkanesulfonic acids of lower molecular weight have remained laboratory curiosities. Recently this laboratory developed a catalytic process for large scale production of either individual or mixed alkanesulfonic acids. This paper describes the preparation of the C_1 to C_4 acids, summarizes published information on their physical and chemical properties, records new information concerning these properties, and suggests potential uses.

THE catalytic method developed for the synthesis of these acids is relatively simple. By use of this process primary and secondary mercaptans, or the corresponding alkyl disulfides, have been oxidized to alkanesulfonic acids of 90 to 100% strength. The over-all equations are:

$$2RSH + 3O_2 \longrightarrow 2RSO_3H$$

$$2R{-}S{-}S{-}R + 5O_2 + 2H_2O \longrightarrow 4RSO_3H$$

The alkyl disulfides are readily available as by-products from the refining of gasoline and various naphthas, or can easily be synthesized from mercaptans. These in turn can be prepared from olefins and hydrogen sulfide by various methods described in the literature.

When alkyl disulfides are employed as the starting materials and care is taken to exclude water from the system, alkanesulfonic anhydrides can be obtained.

$$2R{-}S{-}S{-}R + 5O_2 \longrightarrow 2RSO_2{-}O{-}SO_2R$$

Laboratory oxidation of dimethyl and diethyl disulfides has yielded products containing up to 80% of the corresponding sulfonic anhydrides.

The oxidation of alkyl disulfides to alkanesulfonic acids is now being carried out successfully on a pilot plant scale, and its translation to commercial scale is expected in the near future. In the operation a mixture of the alkyl disulfides and the appropriate amount of water are oxidized in the presence of the catalyst until the transformation to sulfonic acids is virtually complete. Few side reactions occur, and yields of technical sulfonic acids approaching the theoretical are obtained.

The process was applied to the preparation of methane- and ethanesulfonic acids, but the chief emphasis was on synthesizing a mixture of acids. Crude alkyl disulfides, averaging approximately two carbon atoms per alkyl group, and consisting chiefly of symmetrical and unsymmetrical methyl, ethyl, and propyl disulfides in all possible combinations, were oxidized to yield a mixture of methane-, ethane-, propane-, and probably some butanesulfonic acids.

PHYSICAL AND CHEMICAL PROPERTIES

The lower alkanesulfonic acids are strong, nonoxidizing acids. With the exception of methanesulfonic acid which melts at

TABLE I. PHYSICAL PROPERTIES OF C_1 TO C_4 ALKANESULFONIC ACIDS

Compound	B.P. °C.	B.P. Mm.	M.P., °C.	Sp. Gr., 25°/40° C.
CH_3SO_3H	122[a]	1.0	+20.0	1.4844
$CH_3CH_2SO_3H$	123[a]	1.0	−17.0	1.3341
$CH_3CH_2CH_2SO_3H$	136	1.0	+7.5	1.2516
$CH_3CH(SO_3H)CH_3$	123[a]	1.0	....	....
$CH_3CH_2CH_2CH_2SO_3H$	147	0.5	−15.2	1.1906

[a] Boiling points obtained in this laboratory. The value for $CH_3CH(SO_3H)CH_3$ (synthesized in this laboratory) is approximate, since some decomposition occurred at that temperature and pressure.